Biophysical Journal Volume 93 November 2007 3324–3337

Mechanisms of Electrically Mediated Cytosolic Ca^{2+} Transients in Aequorin-Transformed Tobacco Cells

V. L. Sukhorukov,* J. M. Endter,* D. Zimmermann,† R. Shirakashi,‡ S. Fehrmann,* M. Kiesel,* R. Reuss,*
D. Becker,§ R. Hedrich,§ E. Bamberg,† Th. Roitsch,¶ and U. Zimmermann*
*Lehrstuhl für Biotechnologie, §Lehrstuhl für Molekulare Pflanzenphysiologie und Biophysik, Julius-von-Sachs-Institut für
Biowissenschaften, and ¶Institut für Pharmazeutische Biology, Universität Würzburg, Würzburg, Germany; †Abteilung für
Biophysikalische Chemie, Max-Planck-Institut für Biophysik, Frankfurt, Germany; and ‡Institute of Industrial Science,
The University of Tokyo, Tokyo, Japan

ABSTRACT Cytosolic Ca^{2+} changes induced by electric field pulses of 50-μs duration and 200–800 V/cm strength were monitored by measuring chemiluminescence in aequorin-transformed BY-2 tobacco cells. In Ca^{2+}-substituted media, electropulsing led to a very fast initial increase of the cytosolic Ca^{2+} concentration reaching a peak value within <100–200 ms. Peaking of $[Ca^{2+}]_{cyt}$ was followed by a biphasic decay due to removal of Ca^{2+} (e.g., by binding and/or sequestration in the cytosol). The decay had fast and slow components, characterized by time constants of ~0.5 and 3–5 s, respectively. Experiments with various external Ca^{2+} concentrations and conductivities showed that the fast decay arises from Ca^{2+} fluxes through the plasmalemma, whereas the slow decay must be assigned to Ca^{2+} fluxes through the tonoplast. The amplitude of the $[Ca^{2+}]_{cyt}$ transients increased with increasing field strength, whereas the time constants of the decay kinetics remained invariant. Breakdown of the plasmalemma was achieved at a critical field strength of ~450 V/cm, whereas breakdown of the tonoplast required ~580 V/cm. The above findings could be explained by the transient potential profiles generated across the two membranes in response to an exponentially decaying field pulse. The dielectric data required for calculation of the tonoplast and plasmalemma potentials were derived from electrorotation experiments on isolated vacuolated and evacuolated BY-2 protoplasts. The electrorotation response of vacuolated protoplasts could be described in terms of a three-shell model (i.e., by assuming that the capacitances of tonoplast and plasmalemma are arranged in series). Among other things, the theoretical analysis together with the experimental data show that genetic manipulations of plant cells by electrotransfection or electrofusion must be performed in low-conductivity media to minimize release of vacuolar Ca^{2+} and presumably other vacuolar ingredients.

INTRODUCTION

Cytosolic Ca^{2+} ($[Ca^{2+}]_{cyt}$) has been recognized as a key second messenger in cellular signaling pathways involved in growth, differentiation, induction of apoptosis and gene expression in both animal and plant cells (1–4). A variety of exogenous stimuli, including oxidative stress, cold, osmotic shock, etc., have been found to induce stimulus-specific kinetics of $[Ca^{2+}]_{cyt}$, also denoted as Ca^{2+} signatures (5–7). For instance, potassium permanganate induces in tobacco cells a characteristic $[Ca^{2+}]_{cyt}$ transient lasting for 1–2 min before the induction of defense (8,9). Furthermore, $[Ca^{2+}]_{cyt}$ oscillations have been found to precede stomatal closure in *Arabidopsis* guard cells (10). There is also evidence in the literature that stimulus-specific Ca^{2+} signatures may control a wide range of adaptive responses in plant cells (11,12).

Cold, osmotic challenge and chemicals are persistent scalar stimuli that can frequently induce an unpredictable cascade of secondary reactions within cells. Therefore, interpretation of data is not always straightforward, i.e., the question of whether $[Ca^{2+}]_{cyt}$ transients are primarily caused by exogenous stimuli often remains open. Induction of $[Ca^{2+}]_{cyt}$ transients by external electric fields does not, a priori, share these drawbacks, because the interactions of (vector) electric fields with cells are based on well-established physical principles (13,14). A further advantage of electric field pulses is that they can be applied with micro- and even nanosecond timing (15). Particularly, the ultrashort electric pulses with a duration in the nanosecond range have recently been found to trigger both extracellular Ca^{2+} influx and release of Ca^{2+} from intracellular stores of human lymphocytes (16,17).

It is well known from the work of Link et al. (18) that $[Ca^{2+}]_{cyt}$-mediated processes in plant cells can also be elicited by a prolonged DC field application. Examples are the activation of MAP kinases and the induction of defense genes (18). Furthermore, Sano et al. (19) have shown that the $KMnO_4$-induced $[Ca^{2+}]_{cyt}$ transients in tobacco cells can be mimicked by applying a train of short electric pulses. Interestingly, the authors found that the electric field-mediated Ca^{2+} signature delayed the cell cycle progression in a manner qualitatively similar to that of potassium permanganate, thus supporting the assumption of a role for calcium as a second messenger in the cell cycle regulation. Despite these promising results, little is known about the mechanisms underlying the transient changes in $[Ca^{2+}]_{cyt}$ induced by external electric field stimuli. This is somewhat surprising because elucidation of these mechanisms has far-reaching implications in plant biotechnology, where pulsed DC and AC fields

---

Submitted April 16, 2007, and accepted for publication July 10, 2007.

Address reprint requests to Ulrich Zimmermann, University of Wuerzburg, Biotechnology Am Hubland, Biozentrum, Wuerzburg D-97074, Germany. Tel.: 49-931-8884508; E-mail: zimmerma@biozentrum.uniwuerzburg.de.

Editor: Raimond L. Winslow.

0006-3495/07/11/3324/14 $2.00

doi: 10.1529/biophysj.107.110783

are successfully used for the production of transgenic and hybrid plants (13,20–22).

One reason for the lack of information about the mechanisms underlying the electrically induced $[Ca^{2+}]_{cyt}$ transients in plant cells is that these cells are extremely inhomogeneous dielectric particles. The cell wall, plasmalemma, cytosol, tonoplast, and vacuolar sap differ markedly in their ionic conductivities and dielectric permittivities. Therefore, electric field-mediated $[Ca^{2+}]_{cyt}$ transients can be induced by Ca^{2+} influx into the cytosol from the external medium as well as by Ca^{2+} efflux from the Ca^{2+}-containing vacuole (23,24).

The contributions of the extracellular and vacuolar Ca^{2+} ions to the field-induced $[Ca^{2+}]_{cyt}$ transients depend on the transmembrane voltages induced across the plasmalemma and the tonoplast, which, in turn, are determined by the dielectric properties of the two membranes and the vacuolar, cytosolic, and external compartments. As shown here for vacuolated BY-2 tobacco protoplasts, the dielectric properties of the various compartments and structural elements can be deduced quite accurately from the electrorotation (ROT) spectra of protoplasts by fitting the data with the three-shell model (TSM) (25), i.e., by taking into account the separate charging of the serially arranged plasmalemma and tonoplast capacitances. Analysis of the dielectric data allowed the calculation of the voltages induced by external fields across the two membranes both in the frequency and time domain. This paved the way to correlate the kinetically distinct components of DC pulse-induced $[Ca^{2+}]_{cyt}$ transients monitored by chemiluminescence with external and vacuolar Ca^{2+} fluxes.

MATERIALS AND METHODS

Cell culture

For measuring field-induced $[Ca^{2+}]_{cyt}$ transients the transgenic tobacco BY-2 cell line (*Nicotiana tabacum* L. cv. Bright Yellow 2, hereafter referred to as BY-2 cells) was used (19,26). BY-2 cells constitutively express apoaequorin protein (27). The cells were maintained by weekly subculture in a modified Linsmaier and Skoog medium (28), containing increased concentrations of KH_2PO_4 (370 mg/L) and thiamine HCl (1 mg/L). This basal medium was supplemented with sucrose (3%) and a synthetic auxin 2,4-dichlorophenoxyacetic acid (0.2 mg/L). The pH was adjusted to 5.8 before autoclaving (29). The BY-2 cell suspension was cultured at 25°C on a rotary shaker at 130 rpm in dim light. The osmolality of the growth medium was adjusted to 230 mOsm and the conductivity to 5.8 mS/cm using the cryoscopic osmometer of Gonotec (Berlin, Germany) and the conductometer of Knick (Berlin, Germany).

Before electropulsing, 1 μM coelenterazine was added to the BY-2 cell culture for 16 h to reconstitute functional aequorin (a Ca^{2+}-sensitive photoprotein) as described elsewhere (30). Coelenterazine (native form) was obtained from Berthold Detection Systems (Pforzheim, Germany) and used as a 5 mM stock solution in methanol. Staining with Trypan blue ((TB) final concentration 0.2%; Sigma, Deisenhofen, Germany) was used for microscopic evaluation of cell viability determined 30 min after electropulsing. For cell wall staining the fluorescent anionic dye Calcofluor white (Sigma) was used.

Preparation of vacuolated and evacuolated protoplasts

Vacuolated protoplasts were prepared from tobacco BY-2 cells as described elsewhere (31,32), with slight modifications. An aliquot of a 5-day-old cell suspension was centrifuged at 800 rpm for 5 min. The pellet was resuspended in a solution containing 430 mM mannitol, 1% cellulose (Onozuka RS, Yakult Honsha, Tokyo, Japan), 0.1% Y-23 pectolyase (Sigma), 1% R-10 macerocyme, 1% BSA, 0.1mM $CaCl_2$, and 10 mM MES (pH 5.8) and maintained 2 h at 25°C under gentle agitation conditions. Protoplasts were washed twice at 800 rpm. The washing solution consisted of 430 mM sucrose, 0.1 mM $CaCl_2$, and 0.1 mM MES (pH 5.8).

Evacuolated protoplasts were prepared as described by Hörtensteiner et al. (33). In brief, protoplasts were first isolated from 3-day-old BY-2 cells using 1% cellulase, 0.1% pectolyase, and 350 mM mannitol, pH 5.5. The protoplast suspension was then subjected to Percoll density gradient centrifugation. Evacuolated protoplasts were collected from the resulting pellet.

Intracellular calcium

An aliquot of BY-2 cell suspension (2.5 ml) was washed twice with salt-free 230 mOsm sorbitol solution and then subjected to two freeze-thaw cycles (−196°C and 20°C). Samples were homogenized using a Tenbroeck tissue grinder (Wheaton Science Products, Millville, NJ). After removal of cell wall fragments by filtration the cell sap was analyzed for Ca^{2+} using an ELEX 6361 flame photometer (Eppendorf, Hamburg, Germany).

Calcium concentration in the whole cell extract was found to be 1.0 ± 0.4 mM ($n = 5$, mean ± SD). As the vacuole occupies >90% of the cell volume these data provide a good estimate of the vacuolar Ca^{2+} concentration.

Electrorotation

ROT spectra of BY-2 protoplasts were measured by using a microstructured four-electrode chamber as described in detail by Kiesel et al. (34) The microstructures consisted of planar arrays of circular electrodes of 60-μm diameter, 140-nm thickness, and 300-μm electrode spacing. Rotating fields were generated by application of four 90° phase-shifted, rectangular voltage signals using the pulse generator HP 8130A (Hewlett-Packard, Boeblingen, Germany). The amplitude was varied between 2.5 and 4.8 V_{PP} (peak-to-peak voltage) and the frequency between 10 kHz and 150 MHz; 50–70 μl of the cell suspension was added to the rotation chamber. The protoplasts were observed by using a BX 50 Olympus microscope (Hamburg, Germany) that was equipped with a charge-coupled device video camera connected to a video monitor. ROT spectra were monitored by decreasing the field frequency in steps (four frequency points per decade). At each field frequency, the rotation speed of single cells located near the center of the chamber was determined using a stopwatch. ROT spectra were normalized to a field strength of 100 V_{PP}/cm. Protoplast radii were determined with a calibrated ocular micrometer. The conductivity of the media was adjusted to the desired value by adding appropriate concentrations of KCl.

Measurements of the field frequency f_{c1} at which maximum antifield cell rotation occurred were performed in a macroscopic four-electrode chamber (sample volume 10 μl; spacing of the planar electrodes ~1.2 mm). The frequency f_{c1} was determined by using the contrarotating fields (CRF) technique introduced by Arnold and Zimmermann (35). The cells were viewed with an inverted Leitz-Labovert microscope through a 100× oil-immersion objective. Cell radii were determined with a calibrated eyepiece micrometer. Conductivity within the chamber was monitored by a conductometer connected to two opposite electrodes.

Pulse generators and chemiluminometer

For electropulsing of BY-2 cell suspensions the Multiporator (Eppendorf) as well as the pulse generator HP-214B (Hewlett-Packard) were used. The Multiporator delivers single exponentially decaying field pulses of up to 1200 V voltage, with a rise time of ~100 ns and a decay time constant of 50 μs, as monitored by means of a digital storage oscilloscope Tektronix TDS 3052 (Wilsonville, OR). For injection of a train of low-voltage rectangular electric pulses (field strength 75–200 V/cm; rise time 20 ns, duration 50 μs, fall time 20 ns) the HP-214B generator was used. The pulse repetition rate of 5 pulses/s was controlled by a function generator (TE 7702, Toellner, Herdecke, Germany).

Before electropulsing, the cells were washed two times with and resuspended in an isotonic (230 mOsm) pulsing solution at a final density of 10^5 cells/ml. The low-conductivity pulsing solution (0.25 mS/cm) consisted of 1.5 mM KCl and 230 mM sucrose. The high-conductivity pulsing solution (5 mS/cm) consisted of 40 mM KCl, and 150 mM sucrose. The pH of pulsing solutions was adjusted to 5.8 by the addition of 1 mM MES. Ca^{2+}-substituted pulsing solutions contained 0.01, 0.1 (standard), or 1 mM $CaCl_2$. Depletion of extracellular Ca^{2+} was achieved by 10-min incubation of BY-2 cells in Ca^{2+}-free pulsing solution supplemented with 3 mM EGTA. After EGTA treatment, the cells were washed twice and suspended in Ca^{2+}-free pulsing solution. In some experiments, KCl was replaced by an equivalent concentration of NaCl or CsCl. An aliquot of the cell suspension (~800 μl) was carefully transferred to a standard commercial electroporation cuvette (Eppendorf) consisting of two plane aluminum electrodes (2 cm^2 area) spaced by $d = 4$ mm. The field strength E_0 applied to the cell sample was calculated as $E_0 = V_0/d$. It should be noted that because of the voltage drop across the oxide layer on the electrode surface the actual field strength exerted on the suspended cells can be somewhat lower (by ~10–20%) than the expected field intensity (13,36).

Chemoluminescence of aequorin in BY-2 cells was measured by means of a luminometer (Sirius Luminometer; Berthold Detection Systems). To this end, an electroporation cuvette was placed into the sample compartment of the chemiluminometer. The cuvette electrodes were connected to the Multiporator by means of copper cables. Chemiluminescence measurements started usually 5–10 s before pulse application. The digitized signals were acquired at a rate of 5 data points/s.

RESULTS

Morphological appearance

The microphotographs in Fig. 1 illustrate the typical appearance of 5-day-old tobacco BY-2 cells. The morphology of the cells was similar to that reported by the literature (29,37). From the figures it is evident that BY-2 cells grow in fairly dense clusters (Fig. 1 *A*). The clustered cells exhibited an irregular shape ranging from nearly spherical (Fig. 1 *B*) to rod-like morphology (Fig. 1, *C* and *D*). They were surrounded by a thin wall as indicated by staining with the fluorescent anionic dye Calcofluor white (Fig. 1, *B* and *D*). Elongated shape was typical for sister cells at the beginning of cell wall division (Fig. 1 *D*). During the later division stages, BY-2 cells become more spherical (Fig. 1 *B*). Fig. 1 *C* shows that the vacuoles occupied almost the entire cell volume. The nucleus and organelles were located within a cavity (*arrow* in Fig. 1 *C*) formed by the vacuolar membrane (tonoplast).

Suspensions of BY-2 cells such as illustrated in Fig. 1, *A–D*, were used for the chemiluminescence measurements of field-induced $[Ca^{2+}]_{cyt}$ transients. The strong aggregation of the BY-2 cells (Fig. 1 *A*), however, did not allow preparation of single cells required for electrorotation measurements. Therefore, isolated protoplasts obtained by enzymatic digestion were used for electrorotation (Fig. 1 *E*).

$[Ca^{2+}]_{cyt}$ transients induced by single DC pulses in the presence of extracellular Ca^{2+}

Control BY-2 cells suspended in medium containing 0.1 mM $Ca^{2+}{}_{ext}$ exhibited a background chemiluminescence level CL_0 of (0.4–0.6) × 10^3 arbitrary units (a.u.). Application of a field pulse of at least 200 V/cm led to an immediate increase of chemiluminescence to a peak value CL_{max} due to an increase in $[Ca^{2+}]_{cyt}$ (Fig. 2 *A*). Peaking of the chemiluminescence was followed by a gradual decay to a final level CL_f of ~10^3 a.u. Generally, CL_f was somewhat higher than the background CL_0 before electropulsing. The decay of the $[Ca^{2+}]_{cyt}$ transients consisted of a fast and slow component that could be fitted by superposition of two exponential functions (Eq. 1):

$$CL(t) = A_1 e^{-t/\tau_1} + A_2 e^{-t/\tau_2} + CL_f, \qquad (1)$$

where A_1 and A_2 are the amplitudes and τ_1 and τ_2 the corresponding time constants of the two decay components. Since the final signal CL_f was much smaller than the peak chemiluminescence, the sum of the amplitudes ($A_1 + A_2$) was nearly equal to the peak value CL_{max}. Typical transient chemiluminescence curves induced by a single DC field pulse of 400 V/cm and 800 V/cm field strength are given in Fig. 2 *A*. A field pulse of 400 V/cm yielded a CL_{max} value of ~10^5 a.u. within ~0.2 s after pulse application (*curve 1* in Fig. 2 *A*). Application of a DC pulse of 800 V/cm field strength

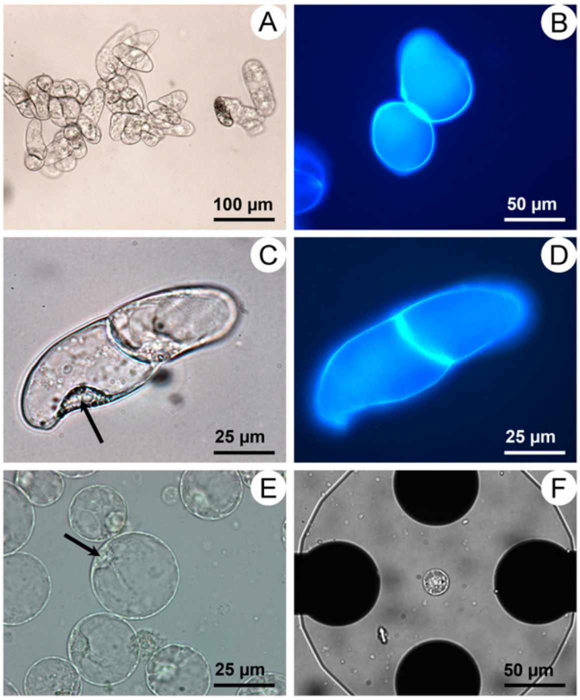

FIGURE 1 Bright-field (*A*, *E*, and *F*), phase contrast (*C*), and fluorescence microphotographs (*B* and *D*) of intact (walled) BY-2 cells (*A–D*) and vacuolated protoplasts (*E* and *F*). In panels *A–D*, BY-2 cells taken from an asynchronous culture are shown. In *B* and *D*, the cells were stained with the fluorescent dye Calcofluor white, which exhibits high affinity to the cell wall (1 mM, excitation wavelength 365 nm). Panels *C* and *E* show that cells and protoplasts contain large central vacuoles separated from the plasmalemma by a thin cytoplasmic layer. The nucleus and organelles are located within a cavity (*arrows*) formed by the tonoplast. Panel *F* illustrates a protoplast located in the center of an ROT chamber that consists of four circular microelectrodes.

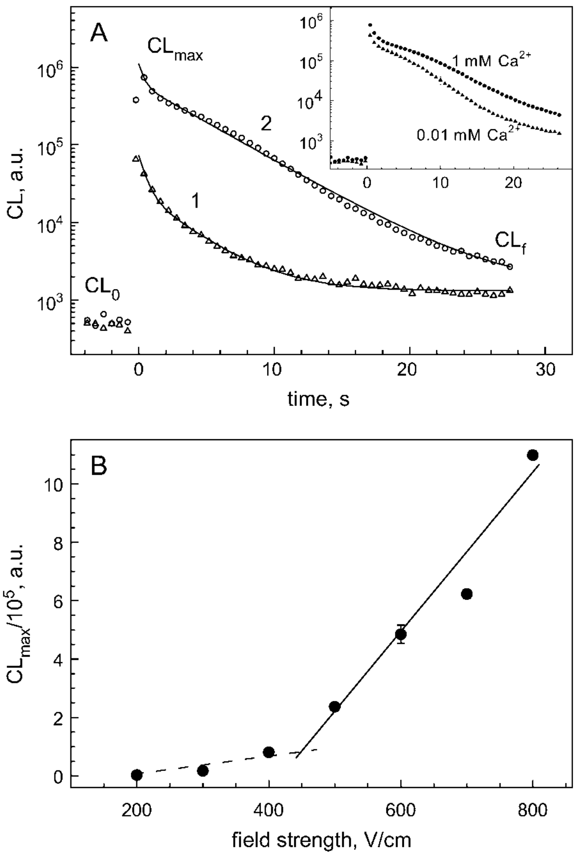

FIGURE 2 Field strength dependence of $[Ca^{2+}]_{cyt}$ transients, measured by chemiluminescence, in aequorin-transformed tobacco BY-2 cells in the presence of 0.1 mM extracellular Ca^{2+}. In panel *A*, triangles and circles denote $[Ca^{2+}]_{cyt}$ transients induced by a field pulse of 400 and 800 V/cm, respectively. In both cases, pulse application (at zero time) led to an instantaneous rise of chemiluminescence from its background level (CL_0) to a peak value (CL_{max}). The continuous curves are fits of the double-exponential function (Eq. 1) to the decay part of $[Ca^{2+}]_{cyt}$ transients. The fitted parameters are given in the text and in Table 1. Inset in panel *A* shows chemiluminescence signals observed in the presence of 0.01 and 1 mM $[Ca^{2+}]_{ext}$ after application of a pulse of 800 V/cm field strength. In panel *B*, CL_{max} values are plotted against the field strength. Note that the slope of the field strength dependence of CL_{max} increases dramatically above 500 V/cm.

resulted in an ~10-fold increase of the CL_{max} value (*curve 2* in Fig. 1 *A*).

Fitting of curve 1 in Fig. 2 *A* by Eq. 1 yielded $A_1 \approx 5 \times 10^4$ a.u. and $A_2 \approx 3 \times 10^4$ a.u. and $\tau_1 \approx 0.4$ s and $\tau_2 \approx 2.8$ s, respectively, for the fast and slow decay component. Raising the field strength to 800 V/cm (Fig. 2 *A*, *curve 2*) increased the amplitudes of both decay components by at least one order of magnitude ($A_1 \approx 5 \times 10^5$ a.u. and $A_2 \approx 6 \times 10^5$ a.u.), whereas their time constants changed—if at all—to a much lesser extent ($\tau_1 \approx 0.5$ s and $\tau_2 \approx 4.7$ s). Table 1 summarizes the mean fitted values of A_1, A_2, τ_1, τ_2, and CL_f of the biphasic decay of the $[Ca^{2+}]_{cyt}$ transients induced by electric pulses of 200–800 V/cm. As shown in Table 1 the squared correlation coefficients (r^2) of the fits were ~0.99. Only in the case of a DC pulse of 200 V/cm, r^2 was somewhat lower (~0.97). The reason for this was the weak chemiluminescence intensity.

Fig. 2 *B* illustrates the dependence of the peak chemiluminescence CL_{max} on the applied field strength. Increasing the field strength from 200 to 400 V/cm resulted in a slight increase of the CL_{max} value, which could be approximated by a straight line (*dashed line*). The slope of the dependence of CL_{max} on field strength increased dramatically above 500 V/cm (*solid line*). Data points above the discontinuity of the CL_{max}-E_0 relation could also be fitted by a straight line. The intersection of the two regression lines gave a field strength of 450 V/cm for the change in slope of the CL_{max}-E_0 relation.

Trypan blue staining performed 30 min after electropulsing showed that application of single DC pulses of up to 800 V/cm intensity did not cause any significant damage to the BY-2 cells in comparison to the control cells (mean ± SE of unstained cells, 96.5 ± 0.2% vs. 95.7 ± 0.5%; $n = 9$). The high viability rates also suggest that the concentrations of Al^{3+} cations solubilized from the anode by electropulsing were too low to induce any detrimental effects on the viability of BY-2 cells. Similarly, various mammalian cell lines tolerate very well electropulsing with short field pulses (microsecond range) in low-conductive sugar-substituted media, such as used in this study (38).

$[Ca^{2+}]_{cyt}$ transients induced by low-intensity pulse trains

In contrast to single pulses (Fig. 2 *B*), chemiluminescence could be induced in BY-2 cells by field strengths <200 V/cm if a train of rectangular pulses was applied in the presence of 0.1 mM Ca^{2+}. As evident from Fig. 3 *A*, application of 5

TABLE 1 Best-fit parameters of the double-exponential function (Eq. 1) to the decay portions of chemiluminescence signals induced by various field strengths in the presence of 0.1 mM $Ca^{2+}{}_{ext}$

Field strength, V/cm*	$A_1/10^3$, a.u.	τ_1, s	$A_2/10^3$, a.u.	τ_2, s	$CL_f/10^3$	r^2
200	2.0 ± 0.2	0.51 ± 0.04	0.6 ± 0.1	5.6 ± 0.8	0.6 ± 0.2	0.967
300	10 ± 2	0.40 ± 0.02	6.7 ± 0.2	2.7 ± 0.1	1.0 ± 0.1	0.998
400	53 ± 5	0.44 ± 0.04	28 ± 2	2.8 ± 0.2	1.5 ± 0.1	0.999
500	171 ± 13	0.52 ± 0.04	65 ± 1	4.1 ± 0.2	1.5 ± 0.1	0.999
600	303 ± 31	0.51 ± 0.05	182 ± 34	4.8 ± 0.1	1.3 ± 0.2	0.999
700	399 ± 15	0.40 ± 0.01	324 ± 9	4.7 ± 0.1	1.1 ± 0.1	0.997
800	518 ± 15	0.45 ± 0.07	581 ± 33	4.7 ± 0.2	0.9 ± 0.1	0.995

*The data are means ± SE of three to four independent measurements. For experimental details, see Fig. 2 legend.

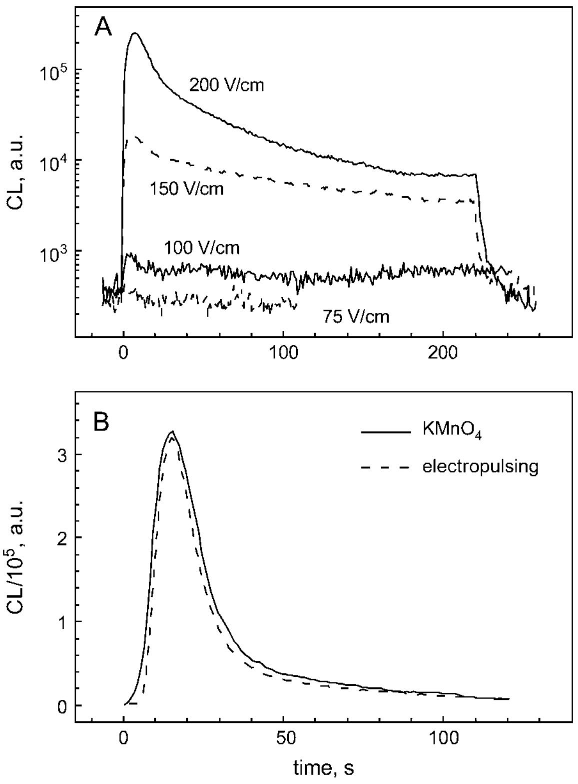

FIGURE 3 Chemiluminescence responses of BY-2 cells to trains of rectangular field pulses ((*A*) 50-μs pulse duration, 5 pulses/s repetition rate) in the presence of 0.1 mM Ca^{2+}. The chemiluminescence recordings shown in panel *A* were obtained on BY-2 cells exposed for ~4 min to pulse trains of the indicated field strengths. Note that a detectable increase of chemiluminescence was observed at a field strength of ≥100 V/cm. Upon switching off the pulse train, the chemiluminescence returned rapidly to the original background level. The solid curve in panel *B* shows a typical $[Ca^{2+}]_{cyt}$ signature in BY-2 cells treated with 50 μM $KMnO_4$. The $KMnO_4$-specific $[Ca^{2+}]_{cyt}$ transients could be mimicked by applying an amplitude-modulated pulse train (*dashed curve*) to BY-2 cells. This was achieved by increasing the amplitude of the train pulses from ~100 to 200 V/cm during the first 20 s of field exposure and subsequent decrease of the amplitudes to nearly zero in the following 80 s.

pulses/s of 100 V/cm strength caused an immediate increase in the chemiluminescence from 350 to ~650 a.u. The value was independent of the time of field exposure (4 min in Fig. 3 *A*). Increase of the field strength of the pulses to 150 V/cm led to a >10-fold increase of CL_{max} (~1.9×10^4 a.u.). After peaking the chemiluminescence declined slightly to a steady level of ~4000 a.u. within ~3 min. A qualitatively similar but more pronounced chemiluminescence response was observed upon exposure of the cells to a train of pulses of 200 V/cm. Independent of the applied field strength, the chemiluminescence decreased rapidly to the background level upon switching off the pulse train (Fig. 3 *A*).

A pulse train whose amplitude increased from 100 and 200 V/cm during the first 20 s of field exposure and subsequently decreased in the next 80 s was used to evoke chemiluminescence transients that were nearly identical to those observed previously with $KMnO_4$ (Fig. 3 *B*; see also Sano et al. (19). Fig. 3 *B* illustrates the applicability of amplitude-modulated pulse trains for an accurate simulation of naturally occurring $Ca^{2+}{}_{cyt}$ transients.

Dependence of $[Ca^{2+}]_{cyt}$ transients induced by a single DC pulse on external Ca^{2+}

Increase of $[Ca^{2+}]_{ext}$ to 1 mM showed no effect on CL_{max} value or on the biphasic decay of the chemiluminescence within the limits of accuracy (see Fig. 2 *A*, *inset*). This finding suggested that CL_{max} has already reached a plateau value at 0.1 mM $[Ca^{2+}]_{ext}$. Consistent with this, a decrease of $[Ca^{2+}]_{ext}$ from 0.1 to 0.01 mM led to a decrease of the CL_{max} value. For instance, at a field strength of 800 V/cm the initial CL_{max} value was reduced from ~10^6 to 0.4×10^6 a.u.

The amplitude, the decay time constants and, in turn, the shape of the electrically induced chemiluminescence transients changed dramatically upon removal of external calcium. For instance, at a field strength of 400 V/cm, CL_{max} dropped to ~10^3 a.u. (*curve 1*, Fig. 4 *A*). Furthermore, the peak value was reached much later (i.e., 1–2 s after electropulsing; Fig. 4 *A*) than in the presence of 0.1 mM $Ca^{2+}{}_{ext}$ (Fig. 2 *A*).

It is also obvious from the figure that the fast decay phase of the chemiluminescence disappeared upon removal of Ca^{2+}. Due to the relatively slow increase in chemiluminescence, the transients in Ca^{2+}-depleted media could be analyzed with a pulse function (Eq. 2) that accounted for both the rising and the decay phase:

$$CL(t) = A(1 - e^{-t/\tau_R})e^{-t/\tau_D} + CL_f, \tag{2}$$

where A is a parameter related with the peak amplitude, CL_{max}, and τ_R and τ_D are the rising and decay time constants, respectively.

Qualitatively similar chemiluminescence transients in Ca^{2+}-free media were observed over the entire range of field strengths. Table 2 summarizes the parameters obtained by fitting Eq. 2 to the $[Ca^{2+}]_{cyt}$ transients measured at field strengths $E \geq 400$ V/cm. Although lower field strengths of 300 and 350 V/cm also induced a detectable increase in chemiluminescence, the fit function did not converge, apparently because of the low signal intensity. Judging by the r^2-values ranging between 0.98 and 0.998, Eq. 2 matches well the kinetics of chemiluminescence. This suggests that in Ca^{2+}-depleted solutions chemiluminescence decreased monoexponentially and not double exponentially as in the presence of $Ca^{2+}{}_{ext}$ (Fig. 2 *A*). As evident from Table 2, increasing field strength from 400 to 800 V/cm resulted in a nearly 20-fold rise of the parameter A from 1.4×10^3 to 26×10^3 a.u., whereas both rising and decay time constants remained unchanged or changed only to a small extent ($\tau_R \approx$ 1–3 s and $\tau_D \approx$ 5–6 s).

Similar to Ca^{2+}-substituted media (Fig. 2 *B*), the CL_{max} values measured in EGTA-treated cells exhibited a strong

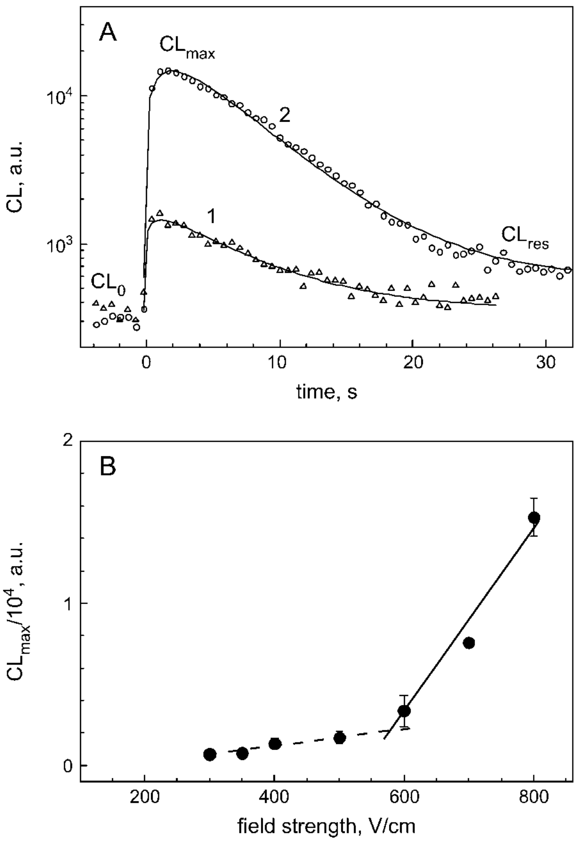

FIGURE 4 Field strength dependence of $[Ca^{2+}]_{cyt}$ transients in EGTA-treated BY-2 cells suspended in Ca^{2+}-free medium. In panel *A*, triangles and circles denote $[Ca^{2+}]_{cyt}$ transients induced by 400 and 800 V/cm, respectively. The continuous curves are best fits of Eq. 2 to the experimental data. The fitted parameters are listed in Table 2. In panel *B*, the dependence of CL_{max} on the applied field strength is shown. Similar to Ca^{2+}-substituted media (Fig. 2 *B*), the field strength dependence of CL_{max} observed in EGTA-treated cells was strongly nonlinear exhibiting a discontinuity at ~580 V/cm.

nonlinear dependence on the applied field strength (Fig. 4 *B*). Between 300 and 500 V/cm, CL_{max} increased only slightly from ~0.7×10^3 to 1.7×10^3 a.u., as indicated by the dashed line. Above 600 V/cm, the slope of the field strength dependence increased dramatically (*solid line*). The intersection of the two regression lines gave a threshold field strength of ~580 V/cm for the change in slope of the CL_{max}-E_0 relation (Fig. 4 *B*). Increase of the external conductivity to 5 mS/cm seemed to shift this threshold field strength to lower values (data not shown).

Effects of external conductivity and monovalent cation substitution on Ca^{2+} transients

The finding that the threshold field strength depended on the external conductivity σ_e in Ca^{2+}-free media prompted us to examine the effect of σ_e on the electrically induced $[Ca^{2+}]_{cyt}$ transients in BY-2 cells in more detail. In the experiment illustrated in Fig. 5, σ_e was adjusted to 0.25 and 5 mS/cm by varying the concentration of KCl (1.5 or 40 mM), while keeping the medium osmolality (230 mOsm) and extracellular Ca^{2+} concentration (0.1 mM) constant. Electropulsing was performed at a field strength of 800 V/cm.

As evident from Fig. 5, σ_e strongly influenced the kinetics of the electrically induced $[Ca^{2+}]_{cyt}$ transients. An increase of σ_e from 0.25 to 5 mS/cm (*curves 1* and *2*, respectively) resulted in an approximately twofold reduction of the initial CL_{max} value from ~5.5×10^5 to ~2.5×10^5 a.u. Increasing σ_e also led to a slower decline of the chemiluminescence, which was apparently due to the lack of the fast decay component (see Table 1). Interestingly, the increase of σ_e rendered the shape of $[Ca^{2+}]_{cyt}$ transients similar to those observed in Ca^{2+}-depleted medium (Fig. 4 *A*). Similar results were obtained when pulses of lower intensity were applied.

We also found that, at a concentration of 1.5 or 40 mM of monovalent cations, the substitution of K^+ by Na^+ or Cs^+ in the pulsing solution affected only slightly—if at all—the $[Ca^{2+}]_{cyt}$ transients in BY-2 cells (data not shown). These findings imply that the external electric conductivity σ_e rather than the kind or the concentration of the monovalent cation was the critical factor determining the electrically induced $[Ca^{2+}]_{cyt}$ transients in BY-2 cells.

Electrorotation of protoplasts

The antifield rotation peak of vacuolated protoplasts was analyzed by means of the CRF technique. This method enables extremely rapid and precise determination of f_{c1}, but it is restricted to low-conductivity media (35). The CRF measurements revealed a strong linear relationship between the product $f_{c1} \times R_1$ and σ_e (Fig. 6 *A*, *inset*), in accordance with Eq. A4. From the straight lines the area-specific membrane capacitance (C_m) and conductance (G_m) could be extracted. Mean values of C_m and G_m were found to be 0.76 ± 0.02 $\mu F/cm^2$ and $G_m = 2.6 \pm 1.4$ mS/cm^2 ($n = 140$), respectively.

TABLE 2 Best-fit parameters of the pulse function (Eq. 2) to the chemiluminescence signals induced by various field strengths in Ca^{2+}-depleted media

Field strength, V/cm*	$A/10^3$, a.u.	τ_R, s	τ_D, s	$CL_f/10^3$	r^2
400	1.4 ± 0.2	2.9 ± 1.5	6.5 ± 0.5	0.4 ± 0.1	0.980
500	2.3 ± 0.3	3.5 ± 1.8	5.4 ± 0.3	0.4 ± 0.1	0.986
600	4.3 ± 0.1	0.9 ± 0.1	6.2 ± 0.1	0.3 ± 0.1	0.995
700	11.3 ± 0.1	1.1 ± 0.1	5.7 ± 0.1	0.4 ± 0.1	0.998
800	26.2 ± 0.3	2.5 ± 0.1	6.0 ± 0.1	0.4 ± 0.1	0.997

*The data are means ± SE of three to four independent measurements. For experimental details, see Fig. 4 legend.

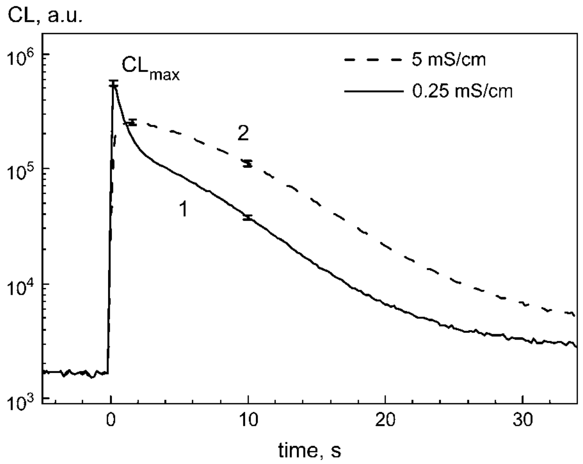

FIGURE 5 The effect of external conductivity σ_e on the electrically induced $[Ca^{2+}]_{cyt}$ transients in BY-2 cells in Ca^{2+}-substituted medium. The solid and dashed curves denote $[Ca^{2+}]_{cyt}$ transients measured at σ_e of 0.25 mS/cm (standard) and 5 mS/cm, respectively, after application of a pulse 800 V/cm field strength and 50 μs duration; σ_e was increased by replacing sucrose by appropriate amounts of KCl in the pulse medium, while keeping the calcium concentration unchanged ($[Ca^{2+}]_{ext} = 0.1$ mM).

By contrast to the CRF technique, ROT spectra could be monitored over a wide range of σ_e ranging from 5 μS/cm to 5 mS/cm. As seen in Fig. 6, *A* and *B*, the ROT spectra exhibited two widely separated anti- and cofield peaks. Fitting the ROT spectra by superposition of two Lorentzian functions (Eq. A3; see Appendix) allowed the determination of the characteristic frequencies f_{c1} and f_{c2} for the anti- and cofield ROT peaks. Plotting the f_{c2} data versus σ_e (Fig. 6 *C*) showed that the cofield peak changed only slightly with increasing σ_e up to 1 mS/cm ($\Omega = 1$–2 radian/s at $f_{c2} = 40$–60 MHz). At a conductivity of 5 mS/cm, the cofield peak moved to frequencies higher than 150 MHz and could not be resolved. Furthermore, over a wide conductivity range (5–200 μS/cm) the cofield rotation was almost constant ($\Omega \approx$ 2 radian/s) and decreased to a value of ~0.8 radian/s at 1 mS/cm. By contrast, antifield rotation exhibited a strong dependency on the external conductivity. The fastest antifield rotation Ω of ~4 radian/s was observed at the low conductivity of $\sigma_e = 5$ μS/cm. With increasing σ_e, the antifield peak rotation decreased gradually to ~1.5 radian/s at 5 mS/cm. Furthermore, plotting the f_{c1} data versus σ_e shows (Fig. 6 *C*) that an increase of the conductivity σ_e from 5 μS/cm to 5 mS/cm shifted the antifield rotation peak from ~2 kHz to 1.6 MHz (Fig. 6, *A* and *B*). The dependency of f_{c1} was not linear. This contrasted the results obtained on evacuolated protoplasts. A plot of the f_{c1} vs. σ_e yielded an almost linear dependency of both parameters (Fig. 7).

The analysis of the ROT spectra of vacuolated and evacuolated BY-2 protoplasts in terms of the single-shell model showed that the cytosolic parameters ε_{cyt} and σ_{cyt} of both cell types did not depend on σ_e as indicated by the plot of the characteristic frequencies f_{c2} vs. σ_e (Figs. 6 *C* and 7). The mean values of the relative dielectric constant, the internal conductivity, and the area-specific membrane conductivity are calculated to be $\varepsilon_{cyt} = 88 \pm 6$, $\sigma_{cyt} = 7.3 \pm 0.4$ mS/cm, and $G_m = 2.6 \pm 1.4$ mS/cm^2 ($n = 38$) for vacuolated protoplasts, and $\varepsilon_{cyt} = 116 \pm 5$, $\sigma_{cyt} = 5.1 \pm 0.2$ mS/cm, and $G_m = 1.6 \pm 0.3$ mS/cm^2 ($n = 26$) for evacuolated protoplasts.

DISCUSSION

We have shown that both amplitude and kinetics of the electrically induced $[Ca^{2+}]_{cyt}$ transients in BY-2 cells measured by chemiluminescence were strongly influenced by the experimental conditions, most notably the field strength, extracellular Ca^{2+}, and medium conductivity. This obviously can be traced back to the multishell structure of the plant cells. The dielectric properties of the two membranes arranged in series as well as of the vacuolar, cytoplasmic, and external compartments determine the charging process of the individual membranes in response to an electric field pulse. The relevant parameters for membrane charging below breakdown can be derived from the analysis of the electrorotation data.

Evaluation of the ROT spectra with the single- and three-shell models

The analysis of the ROT data of evacuolated BY-2 protoplasts in terms of the single-shell model show that the C_m value of evacuolated protoplasts does not depend on external conductivity (Fig. 7). An average C_m value of 0.65 ± 0.01 μF/cm^2 ($n = 26$) was observed over the entire conductivity range. By contrast, the C_m values of vacuolated protoplasts apparently changes strongly with the external conductivity σ_e. At high conductivities (i.e., 0.2–5 mS/cm; Fig. 6 *B*) a C_m value of 0.41 ± 0.01 μF/cm^2 ($n = 22$ cells) is calculated. This value is in agreement with the C_m values of plant cells published in the literature (0.24–0.48 μF/cm^2), which were usually by a factor of 2 or more smaller than those derived for animal cells (0.8–1 μF/cm^2) (39–41). Toward low conductivities (i.e., 5–50 μS/cm) the C_m value of vacuolated BY-2 protoplasts increases substantially (0.60 ± 0.02 μF/cm^2; $n = 16$; see Fig. 6 *A*). An even larger C_m value in the low-conductivity range is derived from the CRF measurements (0.76 ± 0.02 μF/cm^2; $n = 140$; see *inset* in Fig. 6 *A*). The increase of the C_m value below 50 μS/cm is also evident from the strongly nonlinear dependence of the characteristic frequency f_{c1} of the antifield-rotation peak on σ_e (Fig. 6 *C*).

The conductivity dependence of C_m can be explained by assuming that the charging of the plasmalemma and the tonoplast is affected differently by σ_e. This assumption is corroborated by the numerical simulations of the ROT spectra using both the single- and the three-shell model (see *dashed* and *solid curves* in Fig. 6 *D*). The ROT spectra were calculated as the imaginary parts of the complex polarizabilities χ given by Eqs. A2 and A5. The parameters by which the

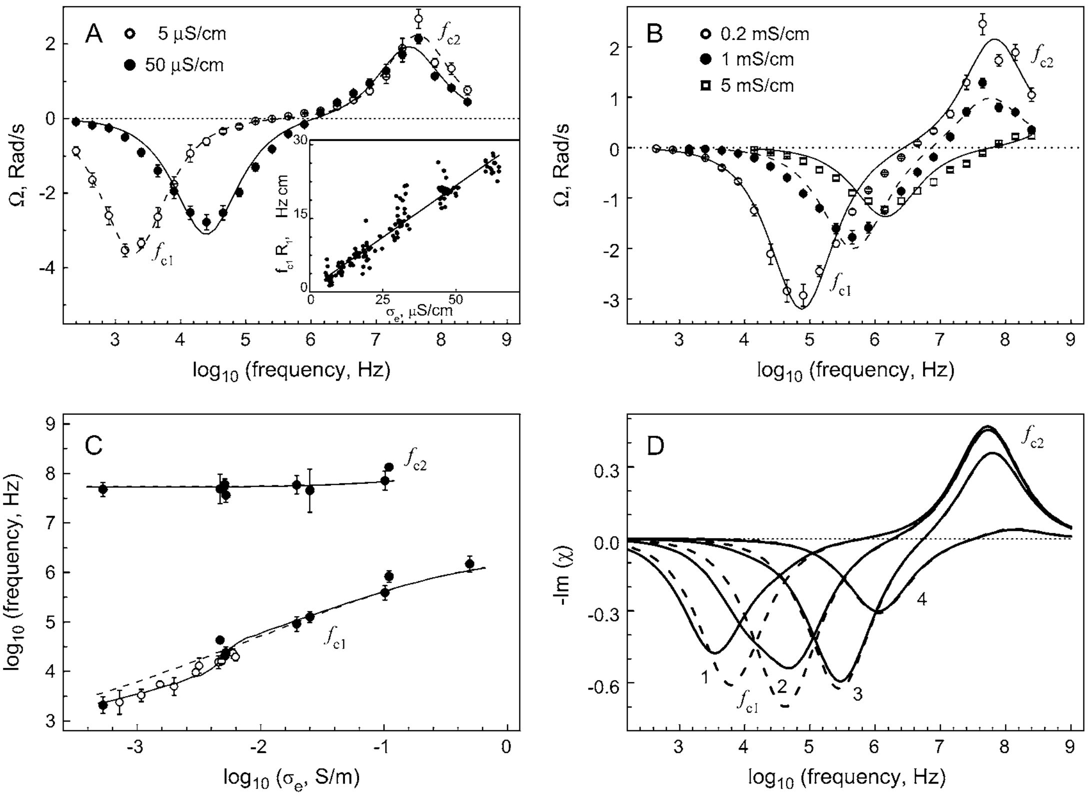

FIGURE 6 Dielectric analysis of vacuolated BY-2 protoplasts by electrorotation. ROT spectra measured at various external conductivities σ_e are shown in panels *A* and *B*. Each spectrum is the mean (± SE) of 9–14 cells. Continuous curves are best fits of Eq. A3 to the data. The characteristic frequencies f_{c1} and f_{c2} denote the anti- and cofield rotation peaks, respectively. Inset in panel *A* shows the radius-normalized f_{c1} data of ~140 cells measured by the CRF technique at very low σ_e between ~5 and 65 μS/cm. Fitting these data to Eq. A4 yields an apparent C_m value of 0.76 ± 0.02 μF/cm^2 and a G_m value of 2.6 ± 1.4 mS/cm^2. In *C*, the f_{c1} and f_{c2} values are plotted versus σ_e. The data were derived either from the ROT spectra (*solid symbols*) or by the CRF method (*open symbols*). The dashed and solid curves were generated, respectively, with the single- and three-shell model, using the parameters listed in Table 3. Note that the three-shell model provides a much better fit to the f_{c1} data than the single-shell model. Theoretical ROT spectra shown in panel *D* were calculated on the basis of the single- and three-shell model (*dashed* and *solid curves*, respectively). ROT speed, given as −Im (χ) (Eqs. A2 and A5) was plotted against Log$_{10}$ (frequency) for σ_e of 0.01, 0.08, 0.64, and 5.12 mS/cm (*curves 1–4*, respectively), using the parameters given in Table 3.

experimental ROT spectra could be approximated are given in Table 3. Curves 1–4 were calculated for σ_e of 10, 80, 640, and 5120 μS/cm.

It is obvious from Fig. 6 *D* that the cofield peaks of the ROT spectra determined experimentally (Fig. 6, *A–C*) could be described quite well by both models over the entire range of σ_e. Both models also described accurately the experimental data obtained for antifield rotation at high conductivity (*curves 3* and *4*). However, toward lower conductivity (<50 μS/cm) the antifield-rotation data could be fitted much better by the three-shell model than by the single-shell model. In contrast to the single-shell model, the three-shell model predicts the shift of the antifield-rotation peak to lower frequencies between 10 and 80 μS/cm (*curves 1* and *2*) as experimentally found (Fig. 6 *C*). The very good agreement between the ROT spectra experimentally determined and the ROT spectra theoretically calculated by the three-shell model over the entire conductivity range suggests that both membranes have a similar area-specific capacitance value (C_p and C_t), but that the contribution of the two capacitances to the electrorotation response of the protoplasts depends on σ_e. At high conductivity both individual membranes are charged. Thus, the area-specific capacitance of the total membrane barrier is ~0.4 μF/cm^2 because the individual membranes are arranged in series. At very low conductivity (e.g., σ_e = 10 μS/cm), only one individual membrane of the barrier is charged. Accordingly the area-specific capacitance increases to 0.60–0.76 μF/cm^2, i.e., to an order of magnitude measured for the single-shelled evacuolated protoplasts.

Induced transmembrane potentials in the frequency and time domains

The very good agreement between the three-shell model and the experimental ROT data measured on vacuolated protoplasts justifies the use of this model for calculations of the transmembrane voltages induced across the plasmalemma (U_p) and tonoplast (U_t). Under the proviso that both U_p and U_t are complex quantities in the frequency domain (see Appendix), their absolute values Abs($\underline{U}_p$) and Abs($\underline{U}_t$) were

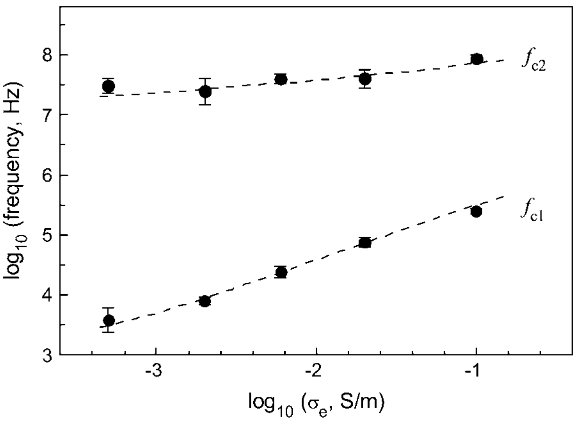

FIGURE 7 Conductivity dependences of the characteristic frequencies f_{c1} and f_{c2} calculated from the ROT spectra of evacuolated BY-2 protoplasts. Each data point represents the mean (± SE) of five to seven cells. The curves were generated by application of the single-shell model, using the mean fitted parameters derived from the ROT spectra of individual protoplasts (see text). Note that the single-shell model matches well the f_{c1} and f_{c2} data of evacuolated protoplasts over the entire conductivity range.

calculated as functions of frequency and conductivity (Fig. 8, *A* and *C*). For calculations the parameters listed in Table 3 were substituted into Eqs. A6 and A7.

At low σ_e the frequency spectra of the plasmalemma voltage U_p shows a single dispersion (Fig. 8 *A*, *curves 1* and *2*), whereas at high σ_e two dispersions occur (Fig. 8 *A*, *curves 3* and *4*). Tonoplast voltages U_t increase above 5 kHz (Fig. 8 *C*). U_t reaches the U_p values at ~100 kHz. Above 1 MHZ the tonoplast is as short-circuited as the plasmalemma. Below 5 kHz U_t is extremely small due to the shielding of the cell interior against the electric field by the insulating plasmalemma. With increase of σ_e the magnitude of U_t increases (*curves 1–4*). Simultaneously the decrease of U_t observed upon short-circuiting of the membrane is shifted to higher frequencies. The frequency spectra of the tonoplast and the plasmalemma voltages allow calculations of the corresponding spectra in the time domain using inverse Laplace transformation (42,43).

TABLE 3 Parameters used for calculations of the ROT spectra, U_p, and U_t for single- and three-shell models

Parameters	Symbol	Value(s)
Common parameters		
Radius of the protoplast	R_1	15 μm
External conductivity (variable)	σ_e	0.01; 0.08; 0.64; 5.12 mS/cm
External permittivity	ε_e	80 ε_0
Applied field strength	E_0	400 V/cm
Single-shell model		
Area-specific membrane capacitance	C_m	0.4 μF/cm^2
Area-specific membrane conductance	G_m	2.6 mS/cm^2
Cytosolic conductivity	σ_{cyt}	7.3 mS/cm
Cytosolic permittivity	ε_{cyt}	88 ε_0
Three-shell model		
Area-specific plasmalemma capacitance	C_p	0.8 μF/cm^2
Area-specific plasmalemma conductance	G_p	5.2 mS/cm^2
Cytosolic conductivity	σ_{cyt}	4 mS/cm
Cytosolic permittivity	ε_{cyt}	80 ε_0
Radius of the vacuole	R_2	0.98 R_1
Tonoplast conductivity	G_t	5.2 mS/cm^2
Tonoplast capacitance	C_t	0.8 μF/cm^2
Conductivity of the vacuolar sap	σ_{vac}	8 mS/cm
Vacuolar permittivity	ε_{vac}	88 ε_0

The pulse-induced $[Ca^{2+}]_{cyt}$ transients were determined on walled BY-2 cells whereas the frequency spectrum was calculated from electrorotation data of vacuolated protoplasts. Transformation of the frequency spectra into the time domain is possible because of the extremely small effects of the porous and highly conductive cell wall on the charging process of membranes (44). Fig. 8, *B* and *D*, illustrate the time courses of the voltages of the plasmalemma U_p and tonoplast U_t in response to an exponentially decaying field pulse of 400 V/cm strength. Obviously, within the first 10 μs, the charging process of the plasmalemma can be described by one exponential function at low conductivity (Fig. 8 *B*; *curves 1* and *2)* and by two exponential ones at high conductivity (*curves 3* and *4*). At time >50 μs, U_p decreases exponentially with a time constant of ~50 μs, in accordance with the decay constant of the applied electric pulse. From the figure it is also obvious that an increase in σ_e led to an increase of the amplitude of the induced voltage U_p. Simultaneously, charging of the plasmalemma is accelerated. As expected from the frequency spectrum in Fig. 8 *C* charging of the tonoplast occurs nonmonotonically, particularly at high σ_e (Fig. 8 *D*, *curves 2–4*). Application of a field pulse leads to a rapid charging of the tonoplast to a maximum value of U_t followed by a slow decline of the voltage. At $t \approx$ 15 μs, when plasmalemma charging reached maximum values, U_t is very low. Interestingly, as in the case of U_p, the magnitude and the rising rate of the U_t transients are affected by σ_e. Both parameters increase with increasing σ_e. Taken together, the induced voltage transients across the plasmalemma (Fig. 8 *B*) exhibit larger magnitudes and longer durations than the corresponding tonoplast potentials (Fig. 8 *D*).

Reversible breakdown of the tonoplast and the plasmalemma

The differences in the charging profiles of the tonoplast and the plasmalemma and their dependency on σ_e have, apparently, a strong impact on the reversible breakdown of the two membranes. The critical field strength required for generation of the membrane breakdown voltage can be estimated from the equation $U = 1.5R_1E_0\cos\vartheta$ (45). The equation is derived for a single-shelled cell and provides that the steady-state voltage across the membrane is reached. Assuming a breakdown voltage of 1 V for a biomembrane (13), a critical field strength of 440 V/cm is calculated. This value

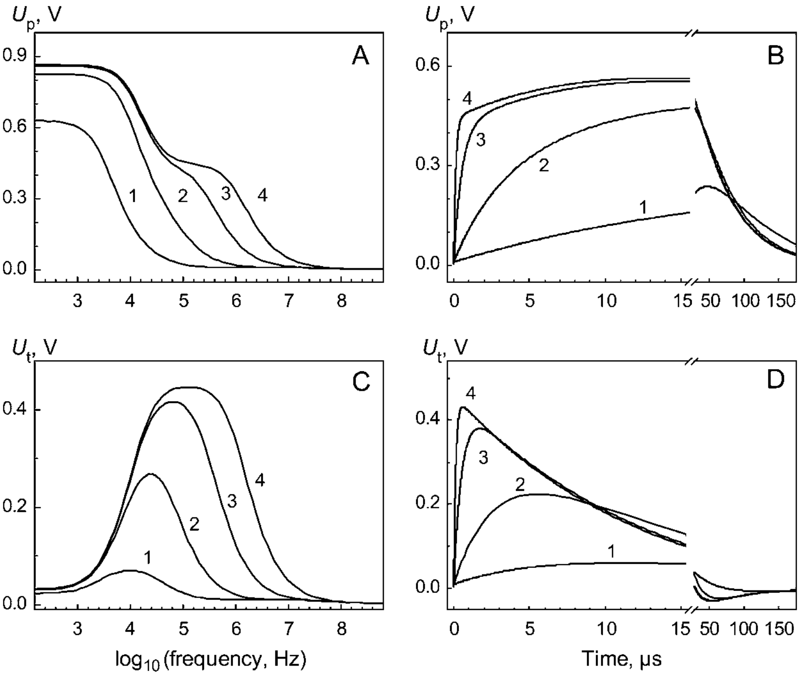

FIGURE 8 Conductivity dependences of the voltages induced across the plasmalemma U_p (*A* and *B*) and tonoplast U_t (*C* and *D*) in the frequency (*A* and *C*) and time (*B* and *D*) domain. Curves 1–4 are plotted for external conductivities σ_e of 0.01, 0.08, 0.64, and 5.12 mS/cm, respectively, using the dielectric parameters of vacuolated protoplasts derived by electrorotation (Table 3). The voltage transients in the time domain (*B* and *D*) were calculated for a field pulse of 400 V/cm decaying exponentially with a time constant of 50 μs.

agrees well with the field strength at which the discontinuity in the CL_{max}-E_0 relation was experimentally observed when measurements were performed in Ca^{2+}-substituted media (Fig. 2 *B*). Inspection of the potential profiles across the tonoplast and the plasmalemma in Fig. 8, *B* and *D*, shows that U_p transients are larger in amplitude and more extended in time than the corresponding U_t transients. This finding suggests that the breakdown voltage of the plasmalemma is reached at a lower external field strength than that of the tonoplast. Thus, the dramatic increase in chemiluminescence above 450 V/cm can most likely be assigned to the breakdown of the plasmalemma. Breakdown of the tonoplast obviously requires an electric field strength of 580 V/cm. This conclusion can be drawn from the measurements in Ca^{2+}-free media (Fig. 4). In the absence of external Ca^{2+} the increase of the chemiluminescence can only be due to vacuolar Ca^{2+} release into the cytoplasm. The electrically induced pathways of Ca^{2+} entry into the cytosol in the presence and absence of extracellular $Ca^{2+}$are illustrated schematically in Fig. 9 (*left* and *right*, respectively).

In the subbreakdown range (i.e., below 450 V/cm), the very weak chemiluminescence responses observed in

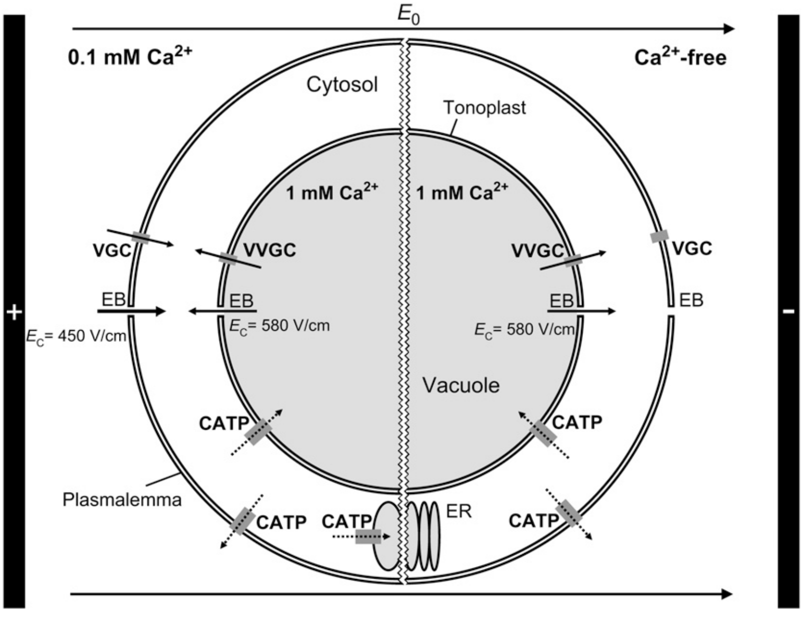

FIGURE 9 Schematic illustration of Ca^{2+} influx and efflux pathways (*solid* and *dashed arrows*, respectively) in a tobacco cell. In the presence of extracellular Ca^{2+} (*left*), external electric field E_0 triggers, via the plasmalemma charging, the Ca^{2+} entry into the cytosol through voltage-gated channels (*VGC*). Above a critical field strength E_c of 450 V/cm, the electric breakdown (*EB*) of the plasmalemma can result in a significant increase of the extracellular Ca^{2+} influx. Similarly, the influx of vacuolar Ca^{2+} into the cytosol can be mediated by the activation of vacuolar voltage-gated channels (*VVGC*) and by the tonoplast breakdown above a critical field strength E_c of 580 V/cm. In the absence of extracellular Ca^{2+} (*right*), only the vacuolar pathways contribute to the electrically mediated $[Ca^{2+}]_{cyt}$ transients. As shown elsewhere (2), energy dependent calcium ATPases (*CATP*) in the plasmalemma, tonoplast, and endoplasmatic reticulum (*ER*) can be involved in the removal of Ca^{2+} from the cytosol (*dashed arrows*).

Ca^{2+}-substituted media seemed to result from the influx of external Ca^{2+} through voltage-gated channels in the plasmalemma, as also proposed elsewhere (18,19). Likewise, the vacuolar Ca^{2+} can also enter the cytosol through voltage-gated channels in the tonoplast (46,47).

Contribution of vacuolar and external [Ca^{2+}] to the chemiluminescence transients

The vacuolar [Ca^{2+}] of BY-2 cells is an order of magnitude higher than the $[Ca^{2+}]_{ext}$ at which most experiments were performed (1 mM vacuolar Ca^{2+} versus 0.1 mM external Ca^{2+}). Therefore, in the first instance one should expect that the increase of $[Ca^{2+}]_{cyt}$ is rather due to field-induced release of vacuolar than of external Ca^{2+} into the cytoplasm because of the large Ca^{2+} gradients across the tonoplast. However, the pronounced reduction of the amplitude of $[Ca^{2+}]_{cyt}$ transients upon removal of external Ca^{2+} demonstrates that vacuolar Ca^{2+} contributes much less to the $[Ca^{2+}]_{cyt}$ transients than external Ca^{2+}. In the light of the above theoretical considerations this finding can be explained straightforwardly by the differences in the amplitude and duration of the generated tonoplast and plasmalemma potentials. According to the potential profiles generated across the tonoplast and plasmalemma (Fig. 8, *B* and D), field-induced Ca^{2+} permeability changes in the plasmalemma must always be larger than those in the tonoplast both in the sub- and above-breakdown range. Furthermore, compared to the tonoplast, the lifetime of the high-permeability state of the plasmalemma must be quite short. This is suggested by the decay kinetics of the chemiluminescence. Aequorin-mediated chemiluminescence requires presence of free Ca^{2+} (12). Thus, the decay rate depends on the one hand from the removal kinetics of free Ca^{2+} from the cytosol (e.g., by binding and/or sequestration of Ca^{2+} by cytosolic macromolecules/organelles and its exclusion from the cytosol by energized transport systems including calcium ATPases (2)) and on the other hand from the supply kinetics of vacuolar and/or external Ca^{2+}, as illustrated schematically in Fig. 9. Measurements of $[Ca^{2+}]_{cyt}$ transients in Ca^{2+} free media have unquestionably shown that the slow decay component must be assigned to Ca^{2+} release from the vacuole into the cytoplasm, because the fast component disappeared (or was too small to be resolved). Disappearance of the fast decay component suggests that this component is predominantly determined by Ca^{2+} influx from the external medium. This means that the influx of external Ca^{2+} decreases rapidly after peaking, whereas release of vacuolar Ca^{2+} continues for some time, thus delaying the decrease of free Ca^{2+} in the cytoplasm. The long-lasting release of vacuolar Ca^{2+} can possibly arise from secondary processes, such as the activation of slow vacuolar type (SV) channels, which are permeable to and activated by Ca^{2+} (48,49). A further interesting finding is that, in the presence of external Ca^{2+}, the fast decay component of the $[Ca^{2+}]_{cyt}$ transients is also not observed at high external conductivity (see Fig. 5). The rise and the decay constant of the $[Ca^{2+}]_{cyt}$ transients were similar to those measured in Ca^{2+} free media (compare Fig. 4). However, the amplitude was higher than in Ca^{2+} free medium. This can only be explained by Ca^{2+} influx from the medium into the cytosol, thus suggesting that at high external conductivity the life span of the high-permeability state of the plasmalemma for Ca^{2+} is of the same order of magnitude as that of the tonoplast.

CONCLUDING REMARKS

In this study the dielectric structure of protoplasts from BY-2 tobacco cells was analyzed by means of the ROT technique. The complex ROT response of vacuolated protoplasts could be explained accurately by a three-shell model accounting for the presence of two serially connected capacitances of the plasmalemma and tonoplast. The three-shell model allowed the calculation of the potential profiles across the plasmalemma (U_p) and tonoplast (U_t) induced by a short DC pulse. The potential profiles explained the field and external conductivity dependence of Ca^{2+} influxes from the vacuole and the external medium into the cytoplasm measured by chemiluminescence. Among other things, the theoretical considerations also show that charging of the tonoplast and the plasmalemma (and thus the breakdown field strength) depends strongly on the external conductivity. The finding that $KMnO_4$-mediated $[Ca^{2+}]_{cyt}$ signatures can be simulated by application of a train of low-intensity field pulses of varying amplitude (Fig. 3) suggests that several secondary processes are apparently involved in the induction of the transients which are difficult to elucidate. Since Ca^{2+} is an important second messenger in both animal and plant cells, electric fields obviously offer an important new tool for controlling cell-signaling pathways for basic research, medical, and biotechnological applications. In general, the experimental findings and theoretical approaches presented here are useful for the development of cell-type specific techniques allowing controlled release of Ca^{2+} from intracellular stores by in situ electromanipulation of organelles in both animal and plant cells. For genetic manipulations of plant cells by electrotransfection or electrofusion it is important to note further that field application must be performed in low-conductivity media to minimize release of Ca^{2+} and presumably other vacuolar ingredients.

APPENDIX: THEORY OF ELECTROROTATION AND MEMBRANE CHARGING BY EXTERNAL ELECTRIC FIELDS

An alternating, rotating or pulsed electric field (E_0) imposed on a cell induces a dipole, μ, and a voltage across the plasmalemma and the membranes of the organelles. The electrostatic interaction of the induced dipole μ with the applied field results in a variety of electrokinetic phenomena (13,25,43,50,51). In a rotating field, the phase shift between E_0 and μ produces a torque that leads to cell rotation (ROT). Comprehensive treatments of ROT and related phenomena (e.g., dielectrophoresis, electrodeformation, etc.) have been given previously (35,52,53). In the case of spherical particles, such as isolated plant protoplasts, the frequency-dependent cell

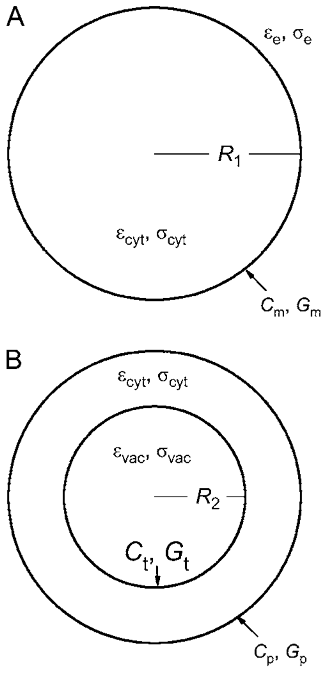

FIGURE 10 Single- and three-shelled spheres as structural models for evacuolated and vacuolated tobacco protoplasts, respectively. R_1 and R_2 denote the external cell and vacuolar radii, respectively; ε and σ are the permittivity and conductivity, respectively. Panels C and G are the capacitance and conductance per unit area, respectively. Subscripts ''e'', ''cyt'', ''t'', and ''vac'' indicate the external medium, cytosol, tonoplast, and vacuolar sap, respectively. Subscripts ''m'' and ''p'' denote the plasmalemma in the single- and three shell model, respectively.

rotation speed $\Omega(f)$ is fully determined by the imaginary part of the complex cell polarizability $\underline{\chi}$, and is given by:

$$\Omega(f) = -\frac{\varepsilon_e E_0^2}{2\eta}\,\mathrm{Im}\underline{\chi}, \tag{A1}$$

where ε_e and η are the permittivity and dynamic viscosity of the external medium, respectively.

In this study, we used the single-shell as well as the three-shell model (Fig. 10) for the interpretation of the ROT spectra of evacuolated and vacuolated protoplasts, respectively. The three-shell model also allowed the calculation of the voltages induced across the plasmalemma (U_p) and tonoplast (U_t) in both time and frequency domains (Fig. 8).

The single-shell model

The expressions for the complex polarizability $\underline{\chi}$ of a single-shelled cell (e.g., evacuolated protoplasts) were derived by using the approach described in detail elsewhere (54). In brief, the particle is assumed to consist of lossless dielectrics with permittivities ε's. The particle is suspended in a lossless medium of permittivity ε_e and subjected to a uniform electric field E_0. Assuming continuity of the electrostatic potential and the normal component of the displacement at the dielectric interfaces yields the following equation for the real polarizability χ:

$$\chi = \frac{R_1 C_m(\varepsilon_{cyt} - \varepsilon_e) - \varepsilon_e\varepsilon_{cyt}}{R_1 C_m(\varepsilon_{cyt} + 2\varepsilon_e) + 2\varepsilon_e\varepsilon_{cyt}}, \tag{A2}$$

where R_1 is the cell radius, C_m is the area-specific membrane capacitance (see Fig. 10). The subscripts ''e'' and ''cyt'' in the permittivities ε-values denote the external medium and cytosol, respectively. For the analysis in the frequency domain (i.e., for the conditions of ROT experiments), the complex polarizability $\underline{\chi}$ was obtained by replacing the real permittivities ε-values, and C_m in Eq. A2 by their complex counterparts: $\underline{\varepsilon} = \varepsilon - j\sigma/\omega$ and $\underline{C}_m = C_m - jG_m/\omega$; ε and σ are the real permittivity and conductivity, respectively, $j = (-1)^{0.5}$ and $\omega = 2\pi f$ is the radian field frequency. The area-specific quantities C_m [F/cm^2] and G_m [S/cm^2] were used because the membrane thickness (~10 nm) is much smaller than the cell radius ($R_1 \approx 15\ \mu$m).

The ROT spectra of single-shelled cells can also be presented as a superposition of two Lorentzian peaks caused by the Maxwell-Wagner dispersions at the outer and inner interfaces of the plasmalemma (13):

$$\Omega(f) = 2A_1\frac{(f/f_{c1})}{1+(f/f_{c1})^2} + 2A_2\frac{(f/f_{c2})}{1+(f/f_{c2})^2}, \tag{A3}$$

where A_1 and A_2 are the amplitudes of the anti- and cofield peaks centered at f_{c1} and f_{c2}, respectively. The two ROT peaks are usually widely separated because of $f_{c1} \ll f_{c2}$. The characteristic frequencies (f_{c1} and f_{c2}) and ROT magnitudes (A_1 and A_2) are affected by the applied field strength, the conductivities, permittivities, and some other parameters of the external medium, membrane, and cytosol (25). Equation A3 was used for the determination of the f_{c1} and f_{c2} values from the experimental ROT spectra. For fitting of the ROT data a MATHEMATICA notebook was devised.

Given that $\sigma_{cyt} \gg \sigma_e \gg \sigma_m$, the single-shell model gives the following relationship between the f_{c1}, R_1, σ_e, and membrane properties:

$$f_{c1} \times R_1 = \frac{\sigma_e}{\pi \times C_m} + \frac{R_1 \times G_m}{2\pi \times C_m}. \tag{A4}$$

Equation A4 was used in this study for the evaluation of the apparent C_m and G_m values from the f_{c1} data obtained by the CRF technique.

The three-shell model

In contrast to the single-shell model, which treats the cell interior as a homogeneous phase, the three-shell model is more realistic because it accounts for the presence of a large tonoplast-bound vacuole of radius R_2 in plant protoplasts (Fig. 10 B). The expressions for the cell polarizability χ, as well as for the voltage drops across the plasmalemma (U_p) and tonoplast (U_t) can easily be found by applying the approach of Jones (54) mentioned above. The following equations for χ, U_p, and U_t were derived using MATHEMATICA:

$$\chi = \frac{C_pR_1\left(\begin{matrix}\varepsilon_{cyt}(2R_1^3(\varepsilon_{cyt}-\varepsilon_e) - R_2^3(2\varepsilon_{cyt}+\varepsilon_e))\varepsilon_{vac} + \\ C_tR_2(R_1^3(\varepsilon_{cyt}-\varepsilon_e)(2\varepsilon_{cyt}+\varepsilon_{vac}) - R_2^3(2\varepsilon_{cyt}+\varepsilon_e)(\varepsilon_{cyt}-\varepsilon_{vac}))\end{matrix}\right) - \varepsilon_{cyt}\varepsilon_e(2(R_1^3-R_2^3)\varepsilon_{cyt}\varepsilon_{vac} + C_tR_2(R_1^3(2\varepsilon_{cyt}+\varepsilon_{vac}) + 2R_2^3(\varepsilon_{vac}-\varepsilon_{cyt})))}{Den}, \tag{A5}$$

$$U_p = \frac{3E_0R_1\varepsilon_{cyt}\varepsilon_e(2\varepsilon_{cyt}\varepsilon_{vac}(R_1^3-R_2^3) + C_tR_2(R_1^3(2\varepsilon_{cyt}+\varepsilon_{vac}) + 2R_2^3(\varepsilon_{vac}-\varepsilon_{cyt})))}{Den}\cos\vartheta, \tag{A6}$$

$$U_{\mathrm{t}}=\frac{9E_0C_{\mathrm{p}}R_1^4R_2\varepsilon_{\mathrm{cyt}}\varepsilon_{\mathrm{e}}\varepsilon_{\mathrm{vac}}}{Den}\cos\vartheta, \tag{A7}$$

where R_1 and R_2 are the cellular and vacuolar radii, respectively (see Fig. 10). C_{p} and C_{t} are the area-specific capacitances of the plasmalemma and tonoplast; θ is the polar angle measured in relation to the field E_0. The subscripts ''e'', ''cyt'', and ''vac'' in the permittivities ε-values denote the external medium, cytosol, and vacuole, respectively. U_{p} and U_{t} are the differences between the electrostatic potentials at the inner and outer boundaries of the plasmalemma and tonoplast, respectively. Note that, U_{p} and U_{t} depend linearly on the cellular and vacuolar radii, respectively. The denominator Den in Eqs. A5–A7 is given by the following expression:

$$Den=\left(\begin{array}{c}2\varepsilon_{\mathrm{cyt}}\varepsilon_{\mathrm{e}}(2\varepsilon_{\mathrm{cyt}}\varepsilon_{\mathrm{vac}}(R_1^3-R_2^3)+C_{\mathrm{t}}R_2(R_1^3(2\varepsilon_{\mathrm{cyt}}+\varepsilon_{\mathrm{vac}})+R_2^3(\varepsilon_{\mathrm{vac}}-\varepsilon_{\mathrm{cyt}})))+\\ C_{\mathrm{p}}R_1\left(\begin{array}{c}2\varepsilon_{\mathrm{cyt}}\varepsilon_{\mathrm{vac}}(R_1^3(\varepsilon_{\mathrm{cyt}}+2\varepsilon_{\mathrm{e}})+R_2^3(\varepsilon_{\mathrm{e}}-\varepsilon_{\mathrm{cyt}}))+\\ C_{\mathrm{t}}R_2(R_1^3(\varepsilon_{\mathrm{cyt}}+2\varepsilon_{\mathrm{e}})(2\varepsilon_{\mathrm{cyt}}+\varepsilon_{\mathrm{vac}})-2R_2^3(\varepsilon_{\mathrm{cyt}}-\varepsilon_{\mathrm{e}})(\varepsilon_{\mathrm{cyt}}-\varepsilon_{\mathrm{vac}}))\end{array}\right)\end{array}\right). \tag{A8}$$

For the analysis in the frequency domain, the complex quantities $\underline{\chi}$, $\underline{U}_{\mathrm{p}}$, and $\underline{U}_{\mathrm{t}}$ were obtained by replacing the real permittivities ε-values, C_{p}, and C_{t} in Eqs. A5–A8 by their complex counterparts: $\underline{\varepsilon}=\varepsilon-j\sigma/\omega$ and $\underline{C}=C-j\,G/\omega$. The theoretical ROT spectra calculated with the three-shell model are illustrated in Fig. 6 *D* (*solid lines*). The voltages induced across the tonoplast U_{t} and the plasmalemma U_{p} in both frequency and time domains are illustrated in the Discussion section (Fig. 8). All calculations were made with the cell parameters given in Table 3, by assuming spherical geometry. Simplified analytical equations for the calculation of the induced membrane voltage in ellipsoidal cells have been derived recently elsewhere (51).

We thank Dr. Stephen Shirley for critical proofreading. We are also very grateful to Lisa Pließ for her excellent technical assistance.

This work was supported by a grant (No. 0313369B) from the Bundesministerium für Bildung und Forschung to U.Z. and E.B.

REFERENCES

1. Knight, H. 2000. Calcium signaling during abiotic stress in plants. *Int. Rev. Cytol.* 195:269–324.
2. Sanders, D., J. Pelloux, C. Brownlee, and J. F. Harper. 2002. Calcium at the crossroads of signaling. *Plant Cell.* 14:401–417.
3. Demaurex, N., and C. Distelhorst. 2003. Apoptosis—the calcium connection. *Science.* 300:65–67.
4. Titushkin, I. A., V. S. Rao, and M. R. Cho. 2004. Mode- and cell-type dependent calcium responses induced by electrical stimulus. *IEEE Trans. Plasma Sci.* 32:1614–1619.
5. Knight, H., A. J. Trewavas, and M. R. Knight. 1996. Cold calcium signaling in Arabidopsis involves two cellular pools and a change in calcium signature after acclimation. *Plant Cell.* 8:489–503.
6. Cessna, S. G., M. A. Messerli, K. R. Robinson, and P. S. Low. 2001. Measurement of stress-induced Ca^{2+} pulses in single aequorin-transformed tobacco cells. *Cell Calcium.* 30:151–156.
7. Mithöfer, A., and C. Mazars. 2002. Aequorin-based measurements of intracellular Ca^{2+}-signatures in plant cells. *Biol. Proc. Online.* 4:105–118.
8. Price, A. H., A. Taylor, S. J. Ripley, A. Griffiths, A. J. Trewavas, and M. R. Knight. 1994. Oxidative signals in tobacco increase cytosolic calcium. *Plant Cell.* 6:1301–1310.
9. Levine, A., R. I. Pennell, M. E. Alvarez, R. Palmer, and C. Lamb. 1996. Calcium-mediated apoptosis in a plant hypersensitive disease resistance response. *Curr. Biol.* 6:427–437.
10. Allen, G. J., S. P. Chu, C. L. Harrington, K. Schumacher, T. Hoffman, Y. Y. Tang, E. Grill, and J. I. Schroeder. 2001. A defined range of guard cell calcium oscillation parameters encodes stomatal movements. *Nature.* 411:1053–1057.
11. Rudd, J. J., and V. E. Franklin-Tong. 2001. Unravelling response-specificity in Ca^{2+} signalling pathways in plant cells. *New Phytol.* 151: 7–33.
12. Lecourieux, D., C. Mazars, N. Pauly, R. Ranjeva, and A. Pugin. 2002. Analysis and effects of cytosolic free calcium increases in response to elicitors in *Nicotiana plumbaginifolia* cells. *Plant Cell.* 14:2627–2641.
13. Zimmermann, U., and G. A. Neil. 1996. Electromanipulation of Cells. CRC Press, Boca Raton, FL.
14. Bobanovic, F., M. D. Bootman, M. J. Berridge, N. A. Parkinson, and P. Lipp. 1999. Elementary $[Ca^{2+}]_i$ signals generated by electroporation functionally mimic those evoked by hormonal stimulation. *FASEB J.* 13:365–376.
15. Schoenbach, K. H., S. J. Beebe, and E. S. Buescher. 2001. Intracellular effect of ultrashort electrical pulses. *Bioelectromagnetics.* 22:440–448.
16. Vernier, P. T., Y. Sun, L. Marcu, S. Salemi, C. M. Craft, and M. A. Gundersen. 2003. Calcium bursts induced by nanosecond electric fields. *BBRC.* 310:286–295.
17. Buescher, E. S., R. R. Smith, and K. H. Schoenbach. 2004. Submicrosecond intense pulsed electric field effects on intracellular free calcium: mechanisms and effects. *IEEE Trans. Plasma Sci.* 32:1563–1572.
18. Link, V. L., M. G. Hofmann, A. K. Sinha, R. Ehness, M. Strnad, and T. Roitsch. 2002. Biochemical evidence for the activation of distinct subsets of mitogen-activated protein kinases by voltage and defense-related stimuli. *Plant Physiol.* 128:271–281.
19. Sano, T., T. Higaki, K. Handa, Y. Kadota, K. Kuchitsu, S. Hasezawa, A. Hoffmann, J. Endter, U. Zimmermann, R. Hedrich, and T. Roitsch. 2006. Calcium ions are involved in the delay of plant cell cycle progression by abiotic stresses. *FEBS Lett.* 580:597–602.
20. Collonnier, U., I. Fock, M.-C. Daunay, A. Servaes, F. Vedel, S. Sijak-Yakovlev, V. Souvannavong, and D. Sihachakr. 2003. Somatic hybrids between *Solanum melongena* and *S. sisymbrifolium*, as a useful source of resistance against bacterial and fungal wilts. *Plant Sci.* 164: 849–861.
21. Sasamoto, H., Y. Wakita, S. Yokota, N. Yoshizawa, T. Katsuki, Y. Nishiyama, T. Yokoyama, and M. Fukui. 2006. Effects of electric cell fusion treatment among leaf protoplasts of *Populus alba* and *Alnus firma* on growth, leaf morphology, and RAPD pattern of eleven acclimatized plants. *In Vitro Cell. Dev. Biol. Plant.* 42:174–178.
22. Valat, L., M. Fuchs, and M. Burrus. 2006. Transgenic grapevine rootstock clones expressing the coat protein or movement protein genes of Grapevine fanleaf virus: characterization and reaction to virus infection upon protoplast electroporation. *Plant Sci.* 170:739–747.
23. Malone, M., R. A. Leigh, and A. D. Tomos. 1991. Concentrations of vacuolar inorganic ions in individual cells of intact wheat leaf epidermis. *J. Exp. Bot.* 42:305–309.
24. Johannes, E., J. M. Brosnan, and D. Sanders. 1992. Parallel pathways for intracellular Ca^{2+} release from the vacuole of higher plants. *Plant J.* 2:97–102.
25. Fuhr, G., and R. Hagedorn. 1996. Cell electrorotation. *In* Electrical Manipulation of Cells. P. T. Lynch and M. R. Davey, editors. Chapman & Hall, NY. 38–70.
26. Takahashi, K., M. Isobe, M. R. Knight, A. J. Trewavas, and S. Muto. 1997. Hypoosmotic shock induces increases in cytosolic Ca^{2+} in tobacco suspension-culture cells. *Plant Physiol.* 113:587–594.

27. Knight, M. R., A. K. Campbell, S. M. Smith, and A. J. Trewavas. 1991. Transgenic plant aequorin reports the effects of touch and cold-shock and elicitors on cytoplasmic calcium. *Nature*. 352:524–526.

28. Linsmaier, E. M., and F. Skoog. 1965. Organic growth factor requirements of tobacco tissue cultures. *Physiol. Plant*. 18:100–127.

29. Nagata, T., Y. Nemoto, and S. Hasezawa. 1992. Tobacco BY-2 cell-line as the ''HeLa'' cell in the cell biology of higher plants. *Int. Rev. Cytol*. 132:1–30.

30. Blume, B., T. Nürnberger, N. Nass, and D. Scheel. 2000. Receptor-mediated increase in cytoplasmic free calcium required for activation of pathogen defense in parsley. *Plant Cell*. 12:1425–1440.

31. Herzog, E., O. Hemmer, S. Hauser, G. Meyer, S. Bouzoubaa, and C. Fritsch. 1998. Identification of genes involved in replication and movement of peanut clump virus. *Virology*. 248:312–322.

32. Sano, T., D. Becker, N. Ivashikona, L. H. Wegner, U. Zimmermann, M. R. G. Roelfsema, T. Nagata, and R. Hedrich. 2007. Plant cells have to pass a K^+ threshold to re-enter cell cycle. *Plant J*. In press.

33. Hörtensteiner, S., E. Martinoia, and N. Amrhein. 1992. Reappearance of hydrolytic activities and tonoplast proteins in the regenerated vacuole of evacuolated protoplasts. *Planta*. 187:113–121.

34. Kiesel, M., R. Reuss, J. Endter, D. Zimmermann, H. Zimmermann, R. Shirakashi, E. Bamberg, U. Zimmermann, and V. L. Sukhorukov. 2006. Swelling-activated pathways in human T-lymphocytes studied by cell volumetry and electrorotation. *Biophys. J*. 90:4720–4729.

35. Arnold, W. M., and U. Zimmermann. 1988. Electro-rotation: development of a technique for dielectric measurements on individual cells and particles. *J. Electrostat*. 21:151–191.

36. Pliquett, U., E. A. Gift, and J. C. Weaver. 1996. Determination of the electric field and anomalous heating caused by exponential pulses with aluminum electrodes in electroporation experiments. *Bioelectrochem. Bioenerg*. 39:39–53.

37. Reisen, D., F. Marty, and N. Leborgne-Castel. 2005. New insights into the tonoplasts architecture of plant vacuoles and vacuolar dynamics during osmotic stress. *BMC Plant Biol*. 5:1–13.

38. Friedrich, U., N. Stachowicz, A. Simm, G. Fuhr, K. Lukas, and U. Zimmermann. 1998. High efficiency electrotransfection with aluminum electrodes using microsecond controlled pulses. *Bioelectrochem. Bioenerg*. 47:103–111.

39. Arnold, W. M., and U. Zimmermann. 1982. Rotating-field-induced rotation and measurement of the membrane capacitance of single mesophyll cells of *Avena sativa. Z. Naturforsch. [C]*. 37:908–915.

40. Glaser, R., G. Fuhr, and J. Gimsa. 1983. Rotation of erythrocytes, plant cells, and protoplasts in an outside rotating electric field. *Stud. Biophys*. 96:11–20.

41. Kaler, K. V. I. S., and T. B. Jones. 1990. Dielectrophoretic spectra of single cells determined by feedback-controlled levitation. *Biophys. J*. 57:173–182.

42. Sukhorukov, V. L., H. Mussauer, and U. Zimmermann. 1998. The effect of electrical deformation forces on the electropermeabilization of erythrocyte membranes in low- and high-conductivity media. *J. Membr. Biol*. 163:235–245.

43. Kotnik, T., and D. Miklavcic. 2006. Theoretical evaluation of voltage inducement on internal membranes of biological cells exposed to electric fields. *Biophys. J*. 90:480–491.

44. Geier, B. M., B. Wendt, W. M. Arnold, and U. Zimmermann. 1987. The effect of mercuric-salts on the electrorotation of yeast-cells and comparison with a theoretical-model. *Biochim. Biophys. Acta*. 900:45–55.

45. Jeltsch, E., and U. Zimmermann. 1979. Particles in a homogeneous electrical-field: model for the electrical breakdown of living cells in a coulter-counter. *Bioelectrochem. Bioenerg*. 6:349–384.

46. Pantoja, O., A. Gelli, and E. Blumwald. 1992. Voltage-dependent calcium channels in plant vacuoles. *Science*. 255:1567–1570.

47. Ping, Z., I. Yabe, and S. Muto. 1992. Identification of K^+, Cl^-, and Ca^{2+} channels in the vacuolar membrane of tobacco cell suspension cultures. *Protoplasma*. 171:7–18.

48. Hedrich, R., and E. Neher. 1987. Cytoplasmic calcium regulates voltage-dependent ion channels in plant vacuoles. *Nature*. 329:833–836.

49. Bewell, M. A., F. J. M. Maathuis, G. J. Allen, and D. Sanders. 1999. Calcium-induced calcium release mediated by a voltage-activated cation channel in vacuolar vesicles from red beet. *FEBS Lett*. 458:41–44.

50. Li, Y., C. Dalton, H. J. Crabtree, G. Nilsson, and K. V. I. S. Kaler. 2006. Continuous dielectrophoretic cell separation microfluidic device. *Lab Chip*. 7:239–248.

51. Maswiwat, K., D. Wachner, R. Warnke, and J. Gimsa. 2007. Simplified equations for the transmembrane potential induced in ellipsoidal cells of rotational symmetry. *J. Phys. D: Appl. Phys*. 40:914–923.

52. Fuhr, G., and P. I. Kuzmin. 1986. Behavior of cells in rotating electric fields with account to surface charges and cell structures. *Biophys. J*. 50:789–795.

53. Pethig, R., V. Bressler, C. Carswell-Crumpton, Y. Chen, L. Foster-Haje, M. E. Garcia-Ojeda, R. S. Lee, G. M. Lock, M. S. Talary, and K. M. Tate. 2002. Dielectrophoretic studies of the activation of human T lymphocytes using a newly developed cell profiling system. *Electrophoresis*. 23:2057–2063.

54. Jones, T. B. 1995. Electromechanics of Particles. Cambridge University Press, New York.